Wall Clutter Mitigation using Discrete Prolate Spheroidal Sequences for Sparse Reconstruction of Indoor Stationary Scenes

Fauzia Ahmad, Jiang Qian*, and Moeness G. Amin

Radar Imaging Lab, Center for Advanced Communications

Villanova University, Villanova, PA 19085

E-mail:{fauzia.ahmad, jiang.qian, moeness.amin}@villanova.edu

Abstract

Detection and localization of stationary targets behind walls is primarily challenged by the presence of the overwhelming electromagnetic signature of the front wall in the radar returns. In this paper, we use the discrete prolate spheroidal sequences to represent spatially extended stationary targets, including exterior walls. This permits the formation of a linear block sparse model relating the range profile and observation vectors. Effective wall clutter suppression can then be performed prior to sparse signal image reconstruction. We consider stepped frequency radar with two cases of frequency measurement distributions over antenna positions. In the first case, the same subset of frequencies is used for each antenna in physical or synthetic aperture arrays, while the other case allows different sets of few frequency observations to be available at different antennas. Using experimental data, we demonstrate that the proposed scheme enables sparsity-based image reconstruction techniques to effectively detect and localize behind-the-wall stationary targets from reduced measurements.

Index Terms

Through-the-wall radar imaging, DPSS, compressive sensing, wall clutter mitigation, sparse reconstruction.

* Jiang Qian is currently with the School of Resources and Environment, University of Electronic Science and Technology of China, Chengdu, China.

I. INTRODUCTION

Detection and localization of stationary targets inside enclosed structures using radio frequency sensors are very pertinent to a variety of civil and military applications, including hostage rescue missions, search-and-rescue operations, and surveillance and reconnaissance in urban environments [1]-[12]. These highly desirable objectives are challenged, amongst other factors, by the presence of clutter caused by the electromagnetic (EM) scattering from the exterior front wall. Front wall returns in ground-based synthetic aperture radar (SAR) systems are typically stronger than those from targets of interest, such as humans [13]. Further, multiple reflections within the boundaries of the front wall or wall reverberations introduce ringing in the radar range profiles, thereby obscuring the weak indoor target returns. Therefore, wall reflections need to be suppressed prior to image formation to reduce clutter and reveal behind-the-wall stationary targets.

A simple but effective method for wall clutter mitigation is background subtraction. If the received signals can be approximated as the superposition of the wall and the target reflections, then subtracting the raw complex data without target (empty scene) from that with the target would remove the wall contributions and eliminate its potentially overwhelming signature in the image. Availability of the empty scene, however, is not possible in many applications. For moving targets, Doppler processing [14] or subtraction of data acquired at different times [15], [16] alleviates this problem and leads to removal of wall reflections as well as suppression of stationary background. However, when the targets of interest are themselves stationary, one must resort to other means to deal with strong and persistent wall reflections.

For conventional imaging based on backprojection, three main approaches have been proposed to deal with strong wall EM reflections without relying on the background scene data

[12], [17]-[19]. In the first approach, the parameters of the front wall, such as thickness and dielectric constant, are estimated from the first wave arrivals [12]. The estimated parameters can be used to model EM wall returns, which are subsequently subtracted from the total radar returns, rendering wall-free signals. Although this scheme is effective, it requires a calibration step, which involves measuring the radar return from a metal plate at the same standoff distance as the front wall under similar, if not identical, operating conditions [20]. The second approach applies a spatial filtering method for wall clutter mitigation [17], which requires measurements from an array aperture that is parallel to the front wall and relies on the wall returns being invariant with changing antenna location. The spatial filter removes the zero spatial frequency component corresponding to the wall return. The third approach recognizes the wall reflections as the strongest component of radar returns, in addition to the invariance of the wall returns across the array aperture [18], [19]. By applying singular value decomposition (SVD) to the measured data matrix, the wall returns occupy low-dimensional subspace and can be captured by the singular vectors associated with the dominant singular values. Accordingly, front wall clutter can be effectively removed by projecting the data measurement vectors at each antenna on the wall orthogonal subspace.

Recently, it has been shown that compressive sensing (CS) techniques can be applied, in lieu of backprojection, to reveal the target positions behind walls [21]-[25]. In so doing, significant savings in data acquisition time can be achieved. Further, producing an image of the indoor scene using few observations can be logistically important, as some of the data measurements in space and frequency can be difficult, or impossible to attain. Both SVD-based and spatial filtering-based wall mitigations in conjunction with CS were considered in [26]. Direct application of these methods to the reduced data volume was shown to provide comparable

performance to their full data volume counterparts. However, this requires specific data collection strategies, which may not be possible logistically, to lead to the desired imaging performance. For stepped frequency radar, this requirement amounts to using the same subset of frequencies for each antenna in physical or synthetic aperture arrays. This ensures that the phase returns of the wall across the antenna elements at each frequency are the same. As a result, the frequency measurement vectors corresponding to the various antenna locations are linearly dependent, leading to a low-dimensional wall subspace. For the case where the frequencies were allowed to differ from one antenna to another, either in a random or preset manner, the wall mitigation algorithms become deprived of the spatial invariance and low-dimensional subspace properties. This is attributed to the fact that the wall phase returns vary across the antennas and the corresponding frequency measurement vectors become linearly independent. In this case, individual range profiles can be first reconstructed using l_1 norm minimization employing a Fourier basis. Then, the data of the missing frequencies are obtained by taking the Fourier Transform of the reconstructed range profile at each antenna. Once the radar returns corresponding to all original frequencies are estimated, wall mitigation can proceed using any conventional wall mitigation method. However, the presence of the wall clutter renders each range profile quite dense and, as such, reduces target detectability [26].

In this paper, we propose an alternate scheme to overcome the shortcomings of the wall clutter mitigation scheme proposed in [26] when a general, non-restricted data collection scheme is employed. Instead of a Fourier basis, we use a dictionary based on discrete prolate spheroidal sequences (DPSS's) to represent the wall returns, which are then captured by block sparsity based approach. This is performed at each available antenna individually. Subtraction of the captured return from the reduced set of measurements at each antenna results in clutter-free data,

thereby permitting the application of CS techniques for image reconstruction.

The rationale behind the use of DPSS dictionary is as follows. Walls are spatially extended targets and the electrical parameters of most walls are frequency dependent, resulting in dispersion and/or distortion of the transmitted signal [27]. This dependency becomes pronounced for higher moisture content of the wall [13]. Further, depending on the signal bandwidth, wall thickness, and wall permittivity, the reverberations may not be separable. Due to the aforementioned reasons, the wall returns may not conform to a point target model. The Fourier basis is considered unsuitable for capturing all of the energy in the wall clutter because it implies the point target model for the underlying phenomenology. Also, the use of finite bandwidth results in "leakage" under the Fourier basis, thereby reducing the scene sparsity. DPSS basis, on the other hand, can well approximate the reverberation signals because of the ability of DPSS's to maximize the energy concentration in a given interval [28].

Unlike the methods in [26], the proposed scheme does not require an array aperture to be parallel to the front wall. It can be applied to a single radar unit as well as to significantly reduced array aperture. The proposed method can be used for both the general case of random selection of the space-frequency variables and the specific simpler case where the same frequencies are used for each available spatial location. Also, the proposed scheme is conceptually similar to the estimate, model, and subtract approach of [12]. However, instead of wall parameter estimation and modeling, we use a DPSS basis to capture the signal energy at ranges in vicinity of the front wall. We note that, unlike the former approach, our proposed approach may treat a target close to the wall as part of the wall reverberation and, consequently, remove its contribution as well from the radar return. On the other hand, it is considered more practical than the estimation and modeling approach as it does not require a calibration step.

Further, the effect of the use of a reduced number of frequency observations on the performance of the estimate, model, and subtract approach for through-the-wall radar imaging has yet to be investigated.

The paper is organized as follows. Section II briefly reviews DPSS's. Through-the-wall signal model is described in Section III. The DPSS based wall clutter suppression scheme is presented in Section IV. CS based image reconstruction using the wall-suppressed data is described in Section V. Supporting experimental results are presented in Section VI, depicting the performance of wall clutter mitigation with DPSS basis under reduced data volume. Section VII provides the conclusion.

II. DISCRETE PROLATE SPHEROIDAL SEQUENCES

Discrete prolate spheroidal sequences are a collection of index-limited sequences that maximize the energy concentration within a given frequency band [28], [29]. The DPSS's constitute a basis for finite-energy signals that are time-limited with their energy concentrated in a given bandwidth. In this paper, since we consider a stepped-frequency signal consisting of K frequencies, we deal with the dual problem to the conventional DPSS's. That is, we are seeking frequency domain sequences, $s[k]$, confined to the frequency index set $[0,1,\dots,K-1]$, whose energy is concentrated in a finite time interval $[-\check{T}, \check{T})$. Since the unambiguous time interval corresponding to a step size of Δf is $[0, 1/\Delta f)$ or equivalently $[-1/2\Delta f, 1/2\Delta f)$, $\check{T}$ lies between 0 and $1/2\Delta f$. Let T be the time $\check{T}$ normalized by $1/\Delta f$ such that $0 < T < 1/2$. Then, exploiting the duality in time and frequency domains, the K-length frequency domain DPSS's are defined as solutions of [29], [30]

$$\boldsymbol{A}\boldsymbol{s}_i = \lambda_i \boldsymbol{s}_i, \qquad i = 0,1,\cdots,K-1 \tag{1}$$

where $\boldsymbol{s}_i$ is a $K \times 1$ vector with elements $s_i[k], k = 0,1,\cdots,K-1$, and λ_i are the eigenvalues of

the matrix $\boldsymbol{A}$, which is given by

$$[\boldsymbol{A}]_{i,k} = \frac{\sin(2\pi T(i-k))}{\pi(i-k)}. \tag{2}$$

The DPSS's are orthonormal on the set $\{0,1,\cdots,K-1\}$.

III. THROUGH-THE-WALL SIGNAL MODEL

Consider an *M*-element linear synthetic aperture radar (SAR) and a wideband stepped-frequency signal, consisting of *K* frequencies equispaced over the desired bandwidth $f_{K-1} - f_0$,

$$f_k = f_0 + k\Delta f, \qquad k = 0,\ldots,K-1 \tag{3}$$

and $\Delta f = \frac{f_{K-1}-f_0}{K-1}$ is the frequency step size. Assume the *M*-element aperture is located along the *x*-axis, parallel to a homogeneous wall, at a nonzero standoff distance. Note that, although the array is assumed to be parallel to the wall, it is not a requirement. Assuming monostatic operation, the wall return at the *m*th antenna location corresponding to the *k*th frequency is given by [31]

$$z_m^w(f_k) = \sum_{l=0}^{L} \sigma_w\, a_l \exp(-j2\pi f_k \tau_w^{(l)}) \tag{4}$$

where σ_w is the complex reflectivity of the wall, L is the number of internal reflections within the wall or wall reverberations, $\tau_w^{(0)}$ is the propagation delay associated with the direct return from the wall, $\tau_w^{(l)},\ l > 0$ are the delays associated with the wall reverberations, and a_l is the path loss factor associated with the *l*th wall return. The decrease in the signal amplitude of the higher order reverberations is accounted for in the corresponding loss factors a_l.

Considering *P* point targets behind the wall and ignoring the target-to-target interactions, the target return at the *m*th antenna corresponding to the *k*th frequency can be expressed as [1][9]

$$z_m^t(f_k) = \sum_{p=0}^{P-1} \sigma_p \exp(-j2\pi f_k \tau_{p,m}) \tag{5}$$

where σ_p is the complex reflectivity of the *p*th target, and $\tau_{p,m}$ is the two-way traveling time

between the *p*th target and the *m*th antenna. Thus, the total baseband signal received by the *m*th antenna corresponding to the *k*th frequency is the superposition of the wall and target returns,

$$z_m(f_k) = z_m^w(f_k) + z_m^t(f_k) \tag{6}$$

The signal received by the *m*th antenna at the K frequencies is arranged into a $K \times 1$ vector $\boldsymbol{z}_m$ as

$$\boldsymbol{z}_m = [z_m(f_0) \quad z_m(f_1) \quad \cdots \quad z_m(f_{K-1})]^T = \boldsymbol{z}_m^w + \boldsymbol{z}_m^t \tag{7}$$

with $z_m(f_k)$ given by (6) and $\boldsymbol{z}_m^w$, $\boldsymbol{z}_m^t$ representing the wall and target contributions at the *m*th antenna, respectively.

IV. WALL CLUTTER MITIGATION UNDER REDUCED DATA VOLUME

A. DPSS Basis

The time-domain equivalent of each of the $K \times 1$ received stepped-frequency signals $\{\boldsymbol{z}_m\}_{m=0}^{M-1}$ is an ensemble of returns concentrated on a number of time intervals within $[-1/2\Delta f, 1/2\Delta f)$. We refer to such signals as "multi-duration signals". We first construct a basis using DPSS's for efficiently capturing the structure of such multi-duration signals.

We divide the unambiguous time $\left[-\frac{1}{2\Delta f}, \frac{1}{2\Delta f}\right)$ into $N = \left\lfloor \frac{2}{\Delta f D} - 1 \right\rfloor$ overlapping intervals of length D, where D is selected to be a multiple of $\frac{1}{(K-1)\Delta f}$. The *n*th time interval is centered at $-\frac{1}{2\Delta f} + \frac{nD}{2}$ and has an extent $\Delta_n = \left[-\frac{1}{2\Delta f} + \frac{nD}{2} - \frac{D}{2}, \ -\frac{1}{2\Delta f} + \frac{nD}{2} + \frac{D}{2}\right]$, $n = 1,2,\cdots,N$. Note that the choice of non-overlapping set of intervals would be inadequate since the radar returns from the various scatterers may not lie exactly on the chosen grid. Let $T = \frac{D\Delta f}{2}$ and $t_n = \left(-\frac{1}{2\Delta f} + \frac{nD}{2}\right)\Delta f$. Consider the $K \times K$ matrix $\boldsymbol{S}_{K,T}$ of K-length frequency domain DPSS's

$$\boldsymbol{S}_{K,T} = [\boldsymbol{s}_0 \quad \boldsymbol{s}_1 \quad \ldots \quad \boldsymbol{s}_{K-1}] \tag{8}$$

with $\{\boldsymbol{s}_i\}_{i=0}^{K-1}$ defined in (1). Forming the $K \times K$ diagonal matrix $\boldsymbol{E}_{t_n}$ as

$$\boldsymbol{E}_{t_n} = \begin{bmatrix} 1 & 0 & \dots & 0 \\ 0 & e^{-j2\pi t_n} & \dots & 0 \\ \vdots & \vdots & \ddots & \vdots \\ 0 & 0 & \dots & e^{-j2\pi(K-1)t_n} \end{bmatrix}, \tag{9}$$

we can define the time-shifted DPSS basis for Δ_n as $\boldsymbol{E}_{t_n}\boldsymbol{S}_{K,T}$. It can be readily shown that $\boldsymbol{E}_{t_n}\boldsymbol{S}_{K,T}$ forms an orthonormal basis for the signals supported on Δ_n in $\mathbb{C}^K$. Moreover, as the first $\lceil 2KT \rceil + 1$ DPSS eigenvalues are close to 1 while the remaining are close to zero, it can be shown that the first $\lceil 2KT \rceil + 1$ time-shifted DPSS's form an efficient signal basis that can efficiently capture the energy of the frequency-domain sequences concentrated on the interval Δ_n [29], [30]. Therefore, we consider the $K \times (\lceil 2KT \rceil + 1)$ matrix $\boldsymbol{\Psi}_n$, comprising the first $\lceil 2KT \rceil + 1$ columns of $\boldsymbol{E}_{t_n}\boldsymbol{S}_{K,T}$ as an efficient basis for signals supported on Δ_n. Thus, the $K \times (\lceil 2KT \rceil + 1)N$ DPSS basis $\boldsymbol{\Psi}$ for the multi-duration signals can be defined as the concatenation of the N time-shifted DPSS bases [30],

$$\boldsymbol{\Psi} = [\boldsymbol{\Psi}_1 \quad \boldsymbol{\Psi}_2 \quad \dots \quad \boldsymbol{\Psi}_N] \tag{10}$$

Using the DPSS basis $\boldsymbol{\Psi}$, the received signal at the mth antenna can be expressed as

$$\boldsymbol{z}_m = \boldsymbol{z}_m^w + \boldsymbol{z}_m^t = \boldsymbol{\Psi}\boldsymbol{\rho}_m^w + \boldsymbol{\Psi}\boldsymbol{\rho}_m^t, \; m = 0,1, \dots, M-1 \tag{11}$$

where $\boldsymbol{\rho}_m^w$ and $\boldsymbol{\rho}_m^t$ are the $(\lceil 2KT \rceil + 1)N$-length coefficient vectors corresponding to the wall and target returns, respectively. It is noted that because of the multi-duration nature of the radar returns, the wall and target contributions, $\boldsymbol{z}_m^w$, $\boldsymbol{z}_m^t$, can be represented using only the columns of $\boldsymbol{\Psi}$ corresponding to the occupied time intervals. Both $\boldsymbol{\rho}_m^w$ and $\boldsymbol{\rho}_m^t$ exhibit a block-sparse structure with the nonzero coefficients occurring in a small number of clusters of size $\lceil 2KT \rceil + 1$.

B. Reduced Data Volume

The data model in (11) involves the full set of measurements made at all M antenna locations using the K frequencies. Assume only $M_1 (< M)$ randomly selected antenna locations are

available for data collection. Let $i_g \in [0,1,\dots,M-1]$, for $g = 0,1,\dots,M_1-1$, be the indices of the employed antenna locations. Consider $\check{\mathbf{z}}_{i_g}$, which is a vector of length $K_1 \ll K$, consisting of elements chosen from $\boldsymbol{z}_{i_g}$ as follows.

$$\check{\mathbf{z}}_{i_g} = \boldsymbol{\varphi}^{(g)}\boldsymbol{z}_{i_g} = \boldsymbol{\varphi}^{(g)}\boldsymbol{z}_{i_g}^{w} + \boldsymbol{\varphi}^{(g)}\boldsymbol{z}_{i_g}^{t} = \check{\mathbf{z}}_{i_g}^{w} + \check{\mathbf{z}}_{i_g}^{t} = \boldsymbol{\varphi}^{(g)}\boldsymbol{\Psi}\boldsymbol{\rho}_{i_g}^{w} + \boldsymbol{\varphi}^{(g)}\boldsymbol{\Psi}\boldsymbol{\rho}_{i_g}^{t} \tag{12}$$

where $\boldsymbol{\varphi}^{(g)}$ is a $K_1 \times K$ measurement matrix constructed by randomly selecting K_1 rows of a $K \times K$ identity matrix. The matrix $\boldsymbol{\varphi}^{(g)}$ determines the reduced set of frequencies corresponding to the i_gth antenna location. Note that the reduced sets of frequencies could either differ from antenna to antenna (as implied in (12)) or be the same for each antenna ($\boldsymbol{\varphi}^{(g)} = \boldsymbol{\varphi}$, $g = 0,1,\dots,M_1-1$).

C. Block Sparse Reconstruction

The goal is to reconstruct the wall contribution at each employed antenna location individually using the reduced measurement vector $\check{\mathbf{z}}_{i_g}$, which can then be subtracted from $\check{\mathbf{z}}_{i_g}$ to obtain the clutter-free radar return at the i_gth antenna. Because of the block sparse nature of $\boldsymbol{\rho}_{i_g}^{w}$ and $\boldsymbol{\rho}_{i_g}^{t}$, we use the block extension of orthogonal matching pursuit (BOMP) to recover the signal component corresponding to the wall [32].

The choice of the number of BOMP iterations is critical to the proposed approach and is directly tied to the number of wall reverberation responses present in the data. The latter is a function of the building material, whose electrical characteristics may not be known in advance. As a result, one can easily under- or over-estimate the number of iterations. Too small a value may not completely capture the wall reverberation, whereas a large enough value may include the returns from targets located at deeper ranges as part of the wall response reconstruction. However, electromagnetic simulations have suggested that even walls composed of non-

homogeneous materials, such as hollow cinder block, have dominant reverberations up to 1.5 m behind the wall [33]. We, therefore, opt for a larger number of iterations and constrain the reconstructed wall clutter support to no more than 1.5 m away from the front face of the wall through inclusion of a purging step in the standard BOMP algorithm. In this way, we can prevent the targets at deeper ranges from being removed along with the wall clutter.

The BOMP algorithm with the purgation step, provided in Table I, will capture the wall contribution only, thereby implying that the output $\hat{\mathbf{z}}_{i_g} \approx \breve{\mathbf{z}}_{i_g}^{w}$. Thus, the target contribution can be obtained by simply subtracting the reconstructed wall contribution in reduced data domain,

$$\breve{\mathbf{z}}_{i_g} - \hat{\mathbf{z}}_{i_g} \approx \breve{\mathbf{z}}_{i_g}^{t} \, . \tag{13}$$

Once the wall clutter has been suppressed individually at each employed antenna location, we can proceed with image formation under reduced data volume.

V. CS BASED IMAGE FORMATION

In this section, we discuss the linear signal model with sensing matrices and the sparse reconstruction scheme for image reconstruction after the wall clutter has been mitigated. Assume that the scene being imaged is divided into $N_x \times N_y$ pixels in crossrange and downrange. Vectorizing the crossrange vs. downrange image into an $N_x N_y \times 1$ scene reflectivity vector $\boldsymbol{\sigma}$ and using the wall clutter-free signal model in (5), we obtain the linear system of equations,

$$\breve{\mathbf{z}}_{i_g}^{t} = \boldsymbol{\Theta}_{i_g} \boldsymbol{\sigma} \tag{14}$$

where the rth element of the qth column of the $K_1 \times N_x N_y$ matrix $\boldsymbol{\Theta}_{i_g}$ is given by

$$\left[\boldsymbol{\Theta}_{i_g}\right]_{r,q} = \exp\left(-j2\pi f_r \tau_{i_g,q}\right), \; r = 0,1,\ldots,K_1 - 1, \; q = 0,1,\ldots,N_x N_y - 1 \tag{15}$$

with $\tau_{i_g,q}$ being the two-way traveling time between the qth pixel and the i_gth antenna. The vector $\boldsymbol{\sigma}$ in (14) is a weighted indicator vector defining the scene reflectivity, i.e., if there is a

Table I. BOMP Algorithm with Purgation Step

Input: number of iterations I, matrix $\boldsymbol{\Sigma} = \boldsymbol{\varphi}^{(g)}\boldsymbol{\Psi}$, measurements $\breve{\mathbf{z}}_{i_g}$, permissible set of wall support indices Ω_w

Initialization: Support set $\Omega_0 = \emptyset$, residual error $\boldsymbol{r}_0 = \breve{\mathbf{z}}_{i_g}$, iteration index $i = 1$

while $i \leq I$

1) $\Omega_i = \Omega_{i-1} \cup \{ \arg\max_n \|\boldsymbol{\Sigma}_n^H \boldsymbol{r}_{i-1}\|_2 \}$, where $\boldsymbol{\Sigma}_n = \boldsymbol{\varphi}^{(g)}\boldsymbol{\Psi}_n$ and the superscript 'H' implies Hermitian operation.

2) $\boldsymbol{r}_i = \breve{\mathbf{z}}_{i_g} - \boldsymbol{\Sigma}_{\Omega_i}\boldsymbol{\Sigma}_{\Omega_i}^{\dagger}\breve{\mathbf{z}}_{i_g}$, where $\boldsymbol{\Sigma}_{\Omega_i}$ denotes the submatrix of $\boldsymbol{\Sigma}$ containing only the columns of $\boldsymbol{\Sigma}$ corresponding to the set Ω_i, and the superscript '†' denotes Pseudoinverse.

3) i=i+1

end

Purgation: $\Omega_I' = \Omega_I \cap \Omega_w$

Output: reconstructed signal, $\hat{\mathbf{z}}_{i_g}\big|_{\Omega_I'} = \boldsymbol{\Sigma}_{\Omega_I'}\boldsymbol{\Sigma}_{\Omega_I'}^{\dagger}\breve{\mathbf{z}}_{i_g}$ and $\hat{\mathbf{z}}_{i_g}\big|_{(\Omega_I')^c} = \mathbf{0}$.

target at the qth pixel, then the value of the qth element of $\boldsymbol{\sigma}$ should be equal to the target reflectivity. Otherwise, it should be zero.

Stacking the wall clutter-free signal samples from all M_1 antenna elements, we obtain the $M_1K_1 \times 1$ measurement vector $\breve{\mathbf{z}}^t$ as

$$\breve{\mathbf{z}}^t = \boldsymbol{\Theta}\boldsymbol{\sigma} \tag{16}$$

where

$$\boldsymbol{\Theta} = \begin{bmatrix} \boldsymbol{\Theta}_{i_0}^T & \boldsymbol{\Theta}_{i_1}^T & \cdots & \boldsymbol{\Theta}_{i_{(M_1-1)}}^T \end{bmatrix}^T. \tag{17}$$

We can recover the sparse vector $\boldsymbol{\sigma}$ from the reduced measurement vector $\breve{\boldsymbol{z}}^t$ in (16) by either solving an l_1 norm minimization problem [34], [35]

$$\hat{\boldsymbol{\sigma}} = \underset{\boldsymbol{\sigma}}{\operatorname{argmin}} \|\boldsymbol{\sigma}\|_1, \text{ subject to } \breve{\boldsymbol{z}}^{\boldsymbol{t}} \approx \boldsymbol{\Theta\sigma} \tag{18}$$

or through use of greedy methods [36]. The latter determine the support of the sparse vector $\boldsymbol{\sigma}$ in an iterative manner, and reconstruct $\boldsymbol{\sigma}$ using the Pseudoinverse. In this work, we use orthogonal matching pursuit (OMP) for the CS based reconstruction [37].

VI. EXPERIMENTAL RESULTS

In this section, we present results of the DPSS based scheme applied to experimental data. We consider both cases of having different frequency measurements at different available antenna locations and also when the same reduced set of frequencies are employed at each of the available antenna locations. For each case of frequency measurement distribution over antenna positions, we provide performance comparison of the proposed scheme with the wall-mitigation based CS approach proposed in [26]. We also compare the performance of the proposed scheme of capturing and subtracting the wall return from the measurements at each antenna when a Fourier basis is used in place of the DPSS basis. Assuming that the unambiguous time $[-1/2\Delta f, 1/2\Delta f)$ is divided into K equally spaced cells of length $\frac{1}{(K-1)\Delta f}$, the signal model, corresponding to (12), under the Fourier basis can be expressed as

$$\breve{\boldsymbol{z}}_{i_g} = \breve{\boldsymbol{z}}_{i_g}^{w} + \breve{\boldsymbol{z}}_{i_g}^{t} = \boldsymbol{\varphi}^{(g)}\boldsymbol{\Psi}_F\boldsymbol{\alpha}_{i_g}^{w} + \boldsymbol{\varphi}^{(g)}\boldsymbol{\Psi}_F\boldsymbol{\alpha}_{i_g}^{t} \tag{19}$$

where $\boldsymbol{\alpha}_{i_g}^{w}, \boldsymbol{\alpha}_{i_g}^{t}$ are the K-length coefficient vectors corresponding to the wall and target returns, respectively, and $\boldsymbol{\Psi}_F$ is a $K \times K$ matrix whose kth column is given by

$$[\boldsymbol{\Psi}_F]_k = \left[e^{-j2\pi f_0 \frac{2kd_r}{c}} \quad \dots \quad e^{-j2\pi f_{K-1} \frac{2kd_r}{c}}\right]^{\boldsymbol{T}}, \quad k = 0,1,\cdots,K-1 \tag{20}$$

with $d_r = c/(2(K-1)\Delta f)$ being the radar range resolution. Given $\check{\mathbf{z}}_{i_g}$, $\boldsymbol{\alpha}_{i_g}^{w}$ can be recovered by using the standard OMP algorithm with a larger number of iterations and a purging step, similar to the one in Table I, at the end to constrain the reconstructed wall clutter support to no more than 1.5 m away from the front face of the wall.

For performance validation, we consider an experiment in which a single target is located behind a solid concrete block wall. We employ the target-to-clutter ratio (TCR) as a performance measure. The TCR is defined as the ratio between the maximum of target pixel value and the average of pixel values in the clutter region [17], [26]

$$TCR = 20\log_{10}\left(\frac{\max_{q\in A_t}|[\hat{\boldsymbol{\sigma}}]_q|}{\frac{1}{Q_c}\sum_{q\in A_c}|[\hat{\boldsymbol{\sigma}}]_q|}\right) \tag{21}$$

where A_t is the target area, A_c is the clutter area, and Q_c is the number of pixels in the clutter area. We select A_t manually in close vicinity of the target (3×4 pixels), whereas A_c is made up of all pixels up to 1.5m behind the front face of the wall directly in front of the array aperture.

A. Experimental Setup

A stepped-frequency SAR system was used for data measurements in the Radar Imaging Lab at Villanova University. The synthetic linear aperture consisted of 93 uniformly spaced elements, with an inter-element spacing of 0.02 m. The aperture was located parallel to a 0.2 m thick solid concrete block wall at a standoff distance of 3.13 m. The stepped-frequency signal comprised 641 frequencies from 1 to 3 GHz, with a step size of 3.125 MHz. A vertical metal dihedral, located at -0.29 m in crossrange (the origin of the coordinate system is placed at the array center) and 2.05 m away from the other side of the front wall, was used as the target. Each face of the dihedral was 0.39 m $\times$ 0.28 m. The side walls were covered with RF absorbing material while the 0.3m thick reinforced concrete back wall was left bare. The distance between the front face

of the back wall and the back face of the front wall is 3.76m. The scene layout is depicted in Figure 1.

The scene to be imaged is chosen to be 4 m × 5.5 m centered at (0, 4.75) m and divided into 33×77 pixels. Figures 2(a) and 2(b) depict the images corresponding to the full raw dataset obtained with backprojection and sparse reconstruction using OMP, respectively. In these and all subsequent reconstructed images, we plot the image intensity on a 35 dB scale, with the maximum intensity value in each image normalized to 0 dB. In addition to the wall reverberation, the antenna ringing is clearly visible in Fig. 2(a) at downranges prior to the front wall. We see that the sparse reconstruction in Fig. 2(b) using OMP with 100 iterations reconstructs only the antenna ringing and wall reverberations, thereby making it necessary to apply wall clutter mitigation in conjunction with CS.

B. Reconstruction Results - Same Set of Reduced Frequencies at Each Employed Antenna

We randomly selected 20% of the antenna locations and randomly chose 20% of the frequencies, which amounts to 4% of the total data volume. The same set of reduced frequencies was employed at each selected antenna location. We reconstructed the scene after application of the subspace projection based CS wall mitigation scheme [26] and the proposed DPSS based wall suppression scheme one hundred times. For each trial, a different random measurement matrix was used to generate the reduced set of measurements, which were then processed for wall clutter mitigation, followed by sparsity-based scene reconstruction. For the DPSS based wall clutter mitigation, the value of the parameter D was chosen to be 5.5 ns and the number of iterations for the modified BOMP was selected as 8.

Figures 3(a) and 3(c) show the sparsity-based reconstructed images obtained after subspace projection based and DPSS based wall clutter mitigation, respectively, both averaged over one

hundred trials. The number of OMP iterations for scene reconstruction was chosen to be 5 in each case. We observe from Fig. 3(a) that, although the target is localized, residual wall clutter and antenna ringing are visible in the image. On the other hand, the DPSS based wall mitigation was successful in removing most of the wall return and the antenna ringing, leading to the 'clean' image in Fig. 3(c) with the target and back wall clearly visible. The loss in image quality for the scheme of [26] compared to that of the proposed DPSS based scheme is also depicted by the corresponding TCR, which takes the respective values of 17.73 dB and 61.33 dB. For comparison, the scene reconstruction result of the proposed scheme with the DPSS basis replaced by Fourier basis for wall clutter mitigation is provided in Fig. 3(b). Although the result with Fourier basis has a TCR of 18.64 dB, which is comparable to that of the subspace based scheme of [26], the reconstruction is quite unstable with the target barely visible. This is expected because the antenna ringing and the wall return do not conform to the point-target model and as such, their energy is not fully captured and removed using the Fourier Basis.

C. Reconstruction Results - Different Set of Reduced Frequencies at Each Employed Antenna

For this more general case, we randomly selected 20% of the antenna locations with a different set of randomly chosen 20% frequencies at each chosen antenna. The number of BOMP and OMP iterations and the value of D were kept the same as for Fig. 3. Figures 4(a), 4(b), and 4(c) show the sparsity-based reconstruction images after wall clutter mitigation corresponding to subspace projection, Fourier basis, and DPSS basis, respectively. Clearly, the DPSS based scheme successfully removed both the antenna ringing and the wall, thereby allowing the subsequent sparse reconstruction to localize the target and the back wall. The corresponding TCR is 72.84 dB. Again, the Fourier basis could not manage to suppress all of the wall clutter

and antenna ringing, and as a result, the reconstruction exhibits a high degree of instability. The corresponding TCR is 16.89dB. For the wall clutter mitigation scheme of [26], the reduced data volume is not sufficient to recover the range profile and all the frequency measurements at each employed antenna location. As a result, the reconstructed image after applying subspace projection based wall mitigation scheme to the full frequency data recovered from the reconstructed range profiles is unable to detect the target.

VII. CONCLUSION

We presented a DPSS based wall clutter mitigation scheme for imaging of stationary targets behind walls using reduced data volume. First, the DPSS basis was used to effectively capture the energy of the wall return at each employed antenna. The reconstructed wall return was subtracted from the measured data at each individual antenna to obtain measurements with reduced wall clutter. This enabled the application of CS techniques for scene reconstruction with fewer observations. Supporting results based on real data experiments demonstrated the superior performance of the proposed scheme over existing schemes when the same set of reduced frequencies were used from each employed antenna and when the reduced sets of frequency measurements were allowed to vary from one antenna to the other.

ACKNOWLEDGMENT

This work was supported by ARO and ARL under contract W911NF-11-1-0536.

REFERENCES

[1] M. G. Amin (Ed.), *Through-the-Wall Radar Imaging*, CRC Press, Boca Raton, FL, 2011.

[2] M. G. Amin (Ed.), "Special issue on Advances in Indoor Radar Imaging," *J. Franklin Inst.*, vol. 345, no. 6, pp. 556–722, Sept. 2008.

[3] M. G. Amin and K. Sarabandi (Eds.), "Special issue on Remote Sensing of Building Interior," *IEEE Trans. Geosci. Remote Sens.*, vol. 47, no. 5, pp. 1270–1420, 2009.

[4] E. Baranoski, "Through-wall imaging: Historical perspective and future directions," *J. Franklin Inst.*, vol. 345, no. 6, pp. 556 – 569, Sept. 2008.

[5] S. E. Borek, "An overview of through the wall surveillance for homeland security," in *Proc. 34th, Applied Imagery and Pattern Recognition Workshop*, vol. 6, Oct. 2005, pp. 19–21.

[6] H. Burchett, "Advances in Through Wall Radar for Search, Rescue and Security Applications," in *Proc. Inst. of Eng. and Tech. Conf. Crime and Security*, London, UK, Jun. 2006, pp. 511–525.

[7] C. P. Lai and R. M. Narayanan, "Ultrawideband random noise radar design for through-wall surveillance," *IEEE Trans. Aerosp. Electronic Syst.*, vol. 46, no. 4, pp. 1716-1730, 2010.

[8] E. F. Greneker, "RADAR flashlight for through-the-wall detection of humans," in *Proc. SPIE – Targets Backgrounds: Charact. Representation IV*, vol. 3375, 1998, pp. 280–285.

[9] M. G. Amin and F. Ahmad, "Wideband synthetic aperture beamforming for through-the-wall imaging," *IEEE Signal Process. Mag.*, vol. 25, no. 4, pp. 110-113, July 2008.

[10] F. Soldovieri and R. Solimene, "Through-wall imaging via a linear inverse scattering algorithm," *IEEE Geosci. Remote Sens. Lett.*, vol. 4, no. 4, pp. 513-517, 2007.

[11] L. P. Song, C. Yu, and Q. H. Liu, "Through-wall imaging (TWI) by radar: 2-D tomographic results and analyses," *IEEE Trans. Geosci. Remote Sens.*, vol. 43, no. 12, pp. 2793–2798, 2005.

[12] M. Dehmollaian and K. Sarabandi, "Refocusing through building walls using synthetic aperture radar," *IEEE Trans. Geosci. Remote Sens.*, vol. 46, no. 6, pp. 1589–1599, 2008.

[13] C. Thajudeen, A. Hoorfar, F. Ahmad, T. Dogaru, "Measured complex permittivity of walls with different hydration levels and the effect on power estimation of TWRI target returns," *Progress in Electromagnetics Research B*, vol. 30, pp. 177–199, 2011.

[14] P. Setlur, M. Amin, and F. Ahmad, "Analysis of micro-Doppler signals using linear FM basis decomposition," in *Proc. SPIE*, vol. 6210, Orlando, FL, May 2006, pp. 62100M.

[15] A. Martone, K. Ranney, and R. Innocenti, "Automatic through the wall detection of moving targets using low-frequency UWB radar," in *Proc. IEEE Int. Radar Conf.*, Washington D.C., May 2010, pp. 39-43.

[16] M. G. Amin and F. Ahmad, "Change detection analysis of humans moving behind walls," *IEEE Trans. Aerosp. Electronic Syst.*, vol. 49, no. 3, pp.1410-1425, Jul. 2013.

[17] Y-S. Yoon and M. G. Amin, "Spatial filtering for wall-clutter mitigation in through-the-wall radar imaging," *IEEE Trans. Geosci. Remote Sens.*, vol. 47, no. 9, pp. 3192–3208, 2009.

[18] F. H. C. Tivive, A. Bouzerdoum, and M. G. Amin, "An SVD-based approach for mitigating wall reflections in through-the-wall radar imaging," in *Proc. IEEE Radar Conf.*, Kansas City, MO, 2011, pp. 519–524.

[19] R. Chandra, A. N. Gaikwad, D. Singh, and M. J. Nigam, "An approach to remove the clutter and detect the target for ultra-wideband through wall imaging," *J. Geophysics and Engineering*, vol. 5, no. 4, pp. 412–419, 2008.

[20] J. Zhang and Y. Huang, "Extraction of dielectric properties of building materials from free-space time-domain measurement," in *Proc. High Frequency Postgraduate Student Colloq.*, Leeds, UK, Sep. 1999, pp. 127–132.

[21] Y.-S. Yoon and M. G. Amin, "Compressed sensing technique for high-resolution radar imaging," *Proc. SPIE*, vol. 6968, pp. 69681A–1–69681A–10, 2008.

[22] Q. Huang, L. Qu, B. Wu, and G. Fang, "UWB through-wall imaging based on compressive sensing," *IEEE Trans. Geosci. Remote Sens.*, vol. 48, no. 3, pp. 1408–1415, 2010.

[23] M. G. Amin, F. Ahmad, and W. Zhang, "A compressive sensing approach to moving target indication for urban sensing," *Proc. IEEE Radar Conf.*, Kansas City, MO, 2011, pp. 509–512.

[24] M. Leigsnering, C. Debes, and A. M. Zoubir, "Compressive sensing in through-the-wall radar imaging," *Proc. IEEE Int. Conf. Acoustics, Speech and Signal Process.*, Prague, Czech Republic, 2011, pp. 4008–4011.

[25] M. G. Amin and F. Ahmad, "Compressive sensing for through-the-wall radar imaging," *J. Electronic Imaging*, vol. 22, no. 3, pp. 030901, Jul. 2013.

[26] E. Lagunas, M. G. Amin, F. Ahmad, and M. Najar, "Joint wall mitigation and compressive sensing for indoor image reconstruction," *IEEE Trans. Geosci. Remote Sens.*, vol. 51, no. 2, pp. 891-906, 2013.

[27] A. Hoorfar and A. Fathy, "Antenna elements, arrays, and systems for through-the-wall radar imaging," in M. Amin (Ed.), *Through-the-Wall Radar Imaging*, CRC Press, 2011, pp. 33-80.

[28] D. Slepian, "Prolate spheroidal wave functions, Fourier analysis, and uncertainty. V – The discrete case," *Bell Syst. Tech. J.* , vol. 57, no. 5, pp. 1371–1430, 1978.

[29] T. Zemen and C. Mecklenbräuker, "Time-variant channel estimation using discrete prolate spheroidal sequences," *IEEE Trans. Signal Process.*, vol. 53, No. 9, pp. 3597-3607, 2005.

[30] M. A. Davenport and M. B. Wakin, "Compressive sensing of analog signals using discrete prolate spheroidal sequences", *Applied and Computational Harmonic Analysis*, vol. 33, no. 3, pp. 438–472, 2012.

[31] M. Leigsnering, F. Ahmad, M. G. Amin, and A. M. Zoubir, "Multipath exploitation in through-the-wall radar imaging using sparse reconstruction," *IEEE Trans. Aerosp. Electronic Syst.*, vol. 50, no. 2, pp. 920–939, Apr. 2014.

[32] Y. Eldar, P. Kuppinger, and H. Bolcskei, "Block-sparse signals: uncertainty relations and efficient recovery," *IEEE Trans. Signal Process.*, vol. 58, no. 6, pp. 3042–3054, 2010.

[33] Available: http://www.navysbir.com/n08_1/N081-075.htm

[34] S. Boyd and L. Vandenberghe, *Convex Optimization*, Cambridge University Press, 2004.

[35] S. S. Chen, D. L. Donoho, and M. A. Saunders, "Atomic decomposition by basis pursuit," *SIAM J. Scientific Computing*, vol. 20, no. 1, pp. 33–61, 1999.

[36] J. A. Tropp, "Greed is good: Algorithmic results for sparse approximation," *IEEE Trans. Inf. Theory*, vol. 50, no. 10, pp. 2231–2242, 2004.

[37] J. A. Tropp and A. C. Gilbert, "Signal recovery from random measurements via orthogonal matching pursuit," *IEEE Trans. Inf. Theory*, vol. 53, no. 12, pp. 4655–4666, 2007.

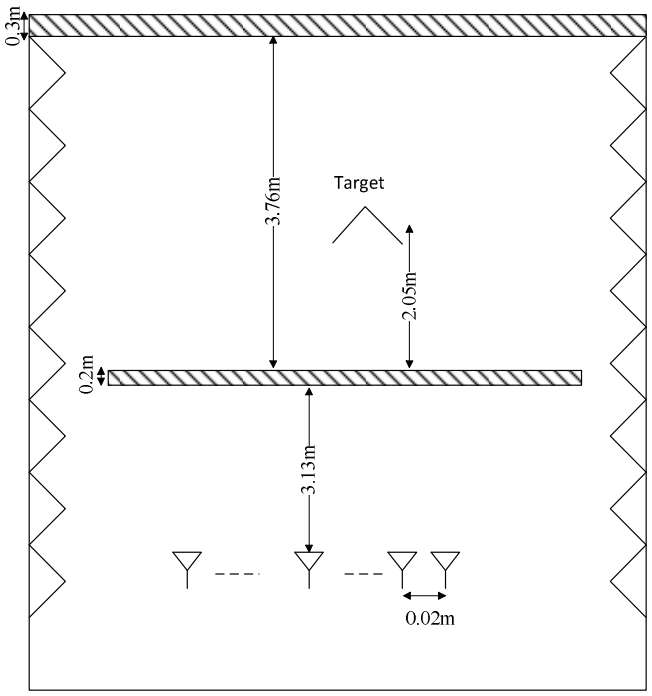

Fig. 1. Scene Layout.

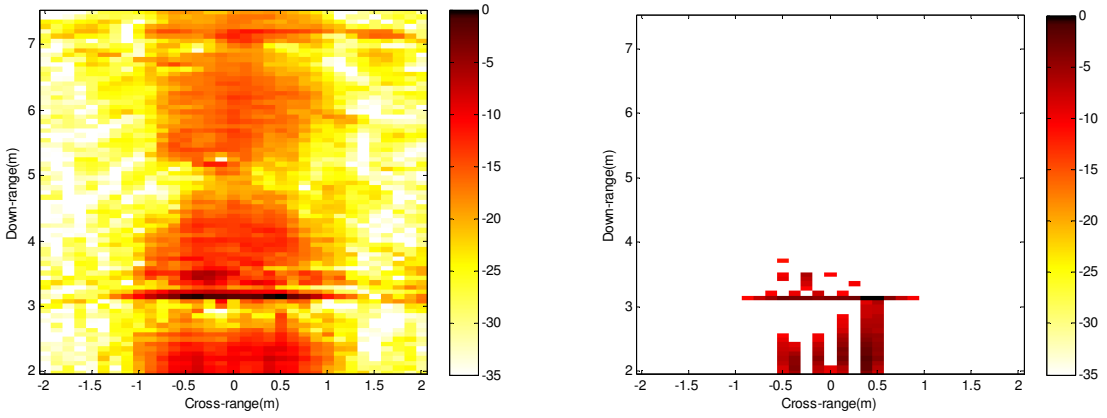

(a) (b)

Figure 2. Reconstructed images using full raw dataset, (a) backprojection, (b) OMP based sparse reconstruction.

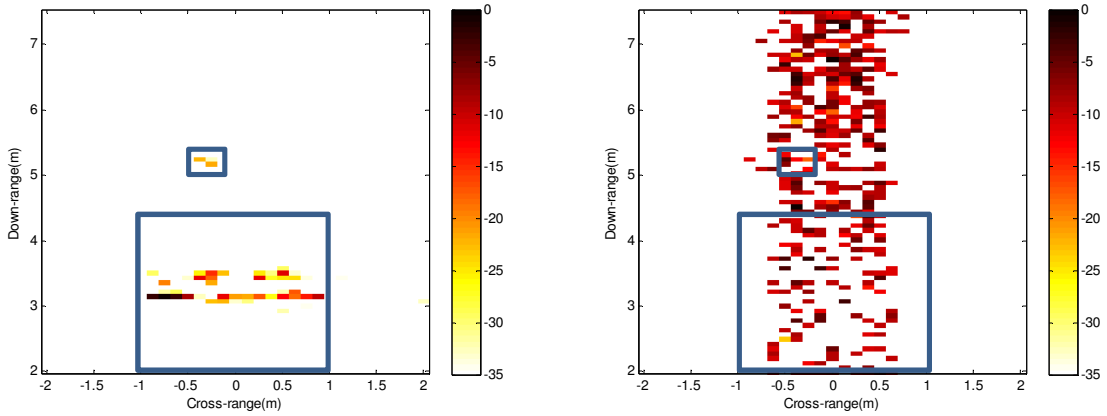

(a) (b)

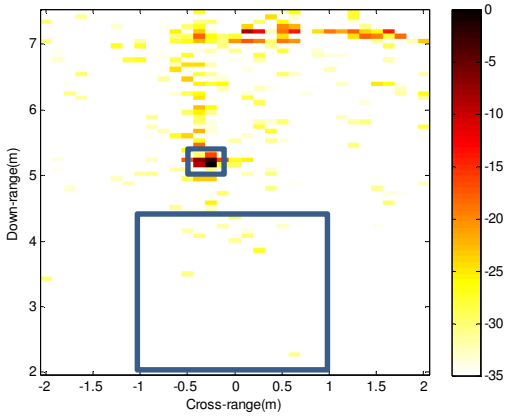

(c)

Figure 3. Sparse reconstruction results using the same reduced frequency set at each employed antenna (4% of the total data volume was employed), (a) subspace projection, (b) Fourier basis, (c) DPSS basis.

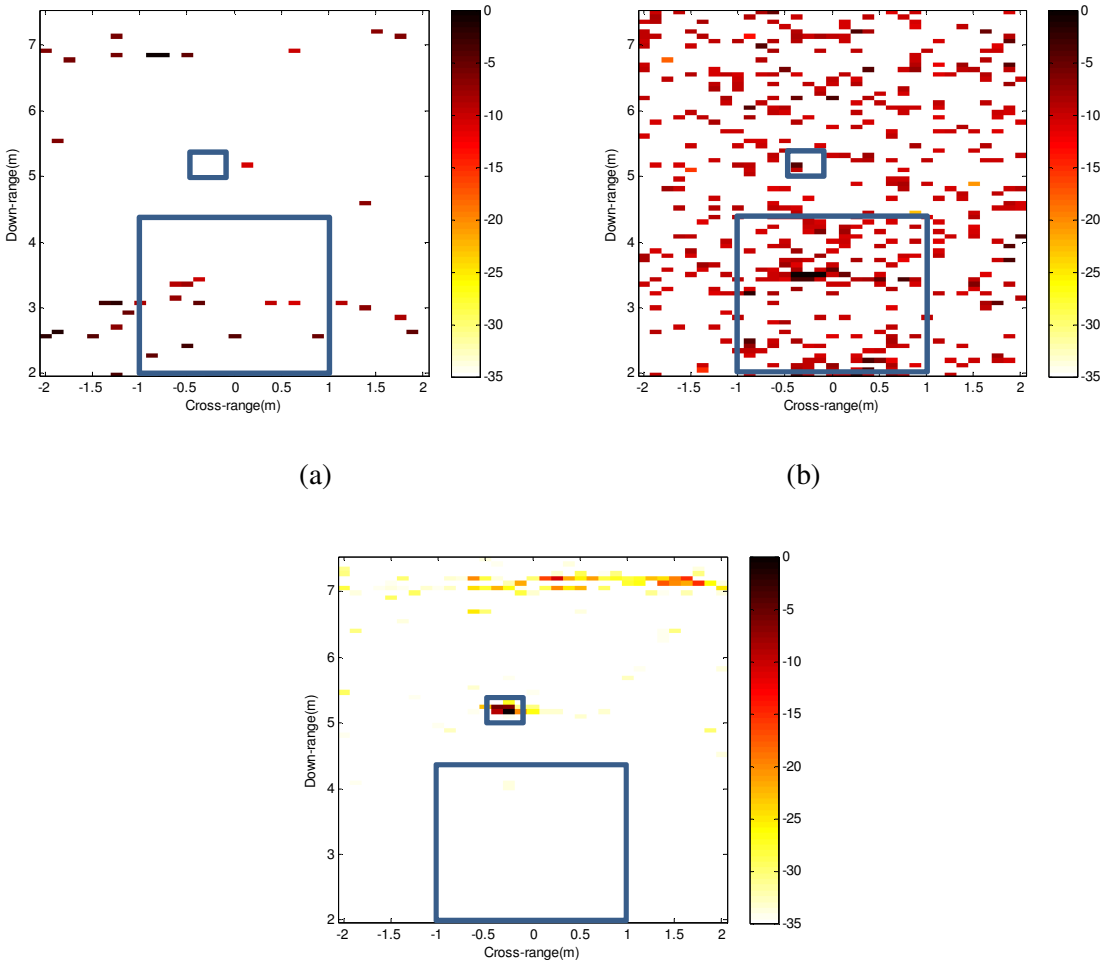

Figure 4. Sparse reconstruction results using different reduced frequency set at each employed antenna (4% of the total data volume was used) (a) subspace projection, (b) Fourier basis, (c) DPSS basis.